JP8.7 DECADAL TEMPERATURE, RAINFALL AND HYDROLOGICAL TRENDS OVER THE GREATER HORN OF AFRICA

J. Bowden, F.H.M. Semazzi*, R. Anyah, B. Onol, A. Tawfik
North Carolina State University, Raleigh, North Carolina

1. INTRODUCTION

Evidence suggests that human activities are influencing the global climate system (IPCC, 1998). Over the Greater Horn of Africa (GHA, Figure 1), there are several physical and biological systems experiencing climate change, such as tropical glacier melt (Hastenrath and Greishar, 1997) and lake surface temperatures warming (O' Reilly et al., 2003), which are known to impact the ecology of the terrestrial and marine environments. Changes in the climate system can also influence human health, economic sustainability and development. In particular the GHA region primary source of revenue is rain-fed agriculture (Serageldin, 1995). Small changes in environmental conditions, in particular rainfall and temperature, may disrupt the productivity of crops and the economic sustainability and development of the GHA region. However, changes such as demographic shifts and land use may also affect the socioeconomic system. Therefore, the relative impact of climate on the socioeconomic sectors is hard to quantify (IPCC, 1998). The objective of this study is to determine through collective evidence that regional changes in rainfall and temperature patterns are occurring over the GHA. Specifically, we will examine trends found over the GHA during the October, November, December season, including observed rainfall and hydrological trends over the Nile Basin, observed and model diagnosed rainfall/temperature trends from a global climate model (CAM2.0.1), and model predicted temperature/rainfall from a global climate model (CCM3) using the IPCC A2 scenario.

2. DATA AND METHODS OF ANALYSIS

2.1 Climate Prediction Center Merged Analysis of Precipitation (CMAP)

Rain-gauge measurement is the traditional

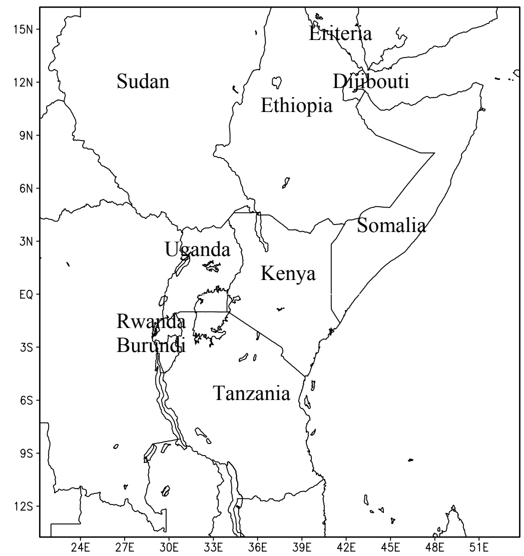

FIG. 1 GHA domain; Analysis is based on the entire domain and subportions of the region.

and oldest method for monitoring rainfall. However, because of practical observational limitations it suffers from numerous gaps in space and time, thus often making its use in climate diagnostic studies less reliable. On the other hand, rainfall estimates based on satellites is spatially and temporally comprehensive when calibrated using rain-gauge measurements (Xie and Arkin 1995). Xie and Arkin (1997) produced a global precipitation data set called CMAP to assist in problems encountered when relying just on rain-gauge observations. CMAP is a global precipitation data set that uses a global 2.5° × 2.5° grid resolution, temporally distributed monthly/pentad from January 1979 – present. This study takes advantage of both the pentad and monthly CMAP data which has been found useful in several previous studies for examining climate variability (Xie et al. 2003).

2.2 Climate Research Unit (CRU TS 2.0)

This study uses surface temperature from the CRU 2.0 dataset. The dataset interpolates monthly surface temperature over the global land surface onto regular 0.5×0.5 grid spacing. The dataset is an extended version of similar data constructed by New et al. (2000). In the present

*Corresponding author address: Fredrick H.M. Semazzi; Department of Marine, Earth and Atmospheric Sciences, North Carolina State University, Raleigh, NC 27695-8208;
email: fred_semazzi@ncsu.edu

study the surface temperature is used to diagnose temperature trends and model evaluation.

2.3 Nile Basin

Investigation of the Nile Basin climate variability uses normalized seasonal discharge along the White Nile and Blue Nile Rivers. The river discharge is calculated from station discharge data during the OND season from 1912 to 1982. We do not include the Main Nile River in this study because the majority of the Main Nile lies outside our region of focus. The White Nile source is Lake Victoria. The Blue Nile source is Lake Tana. Knowledge of the source regions will be important when discussing the results.

2.4 NCAR-CAM2.0.1 Model

The NCAR Community Atmosphere model version 2.0.1 (CAM.2.0.1) was used to generate the 50-year ensemble consisting of 15 realizations. The simulations were perfrormed by NCAR Climate Variability Working Group. The model is a T41 (approximately 2.8°×2.8° horizontal grid spacing) spectral eulerian model with 26 vertical levels. Monthly varying sea-surface temperatures and sea ice are used as lower boundary forcing for the model. The SST and Sea Ice data comprise of analyzed monthly mid-point mean values of SST and ice concentration for the period 1949-2001. The dataset blends together the global Hadley Center Ice and Sea Surface Temperature (HADISST) dataset prior to 1981 and the Smith/Reynolds EOF dataset for post-1981 period. The governing equations are solved using the spectral method in the horizontal, while finite differencing is used for vertical discretization. CAM2.0.1 uses a hybrid vertical coordinate following Simmons and Stufing (1981), which is retain following at the earth's surface but reduces to pressure coordinate at some point above the surface. The cumulus parameterization scheme for deep convection is based on Zhang and McFarlane (1995). The model also has enhanced physics that includes prognostic treatment of cloud-condensed water to deal more realistically with condensation and evaporation due to large scale forcing. Explicit representation of fractional land and sea-ice coverage is adopted in CAM2.0.1 unlike the earlier versions of the NCAR global atmospheric model (the CCM series) that uses a simple land-ocean-sea ice mask to define the underlying surface of the model. Detailed description of NCAR CAM2.0.1 series can be accessed online at the NCAR website.

The ensemble data used in the present study comprises of 50-year simulation 15 realizations. The simulations were performed at NCAR. Perturbing the initial conditions generated the ensemble members. Details of the ensemble simulations can be found online at the NCAR-Climate Variability website (http//:www.ucar.edu). This study takes advantage of the large ensemble size to diagnose the GCM in simulating the climate of the GHA region and trends in rainfall and temperature using empirical orthogonal functions. It is often not possible to generate such large GCM ensemble size, due to the prohibitive computation costs involved.

2.5 NCAR/NASA-CCM3

The CCM3 described here is essentially the same as the eulerian version of NCAR-CCM3, except it uses the mass conserving finite volume dynamics (Lin and Rood, 1996; Lin et al., 2004). The horizontal resolution is based on 1° latitude × 1.25° longitude grid coordinates. Hybrid vertical coordinate system is used with a total of 18 vertical levels. The ensemble generated by the finite volume version of NCAR/NASA-CCM3 consists of a control simulation (1961-1990) and projection based on A2 scenerio (2071-2100) (IPCC, 2001). The simulations were performed at the International Center for Theoretical Physics (ICTP). The ensemble was run using observed SSTs, sea ice distribution, GHGs and aerosol forcing. The ensemble was initialized with climatological January atmospheric fields. A detailed description of NCAR/NASA-CCM3 can be found in Lin and Rood (1996) and Lin et al., (2004), while the ensemble simulation is described in Coppola and Giorgi (2005).

2.6 Empirical Orthogonal Functions (EOF)

EOF is a statistical tool that compresses geophysical data fields in space and time. The technique allows us to explain the variance-covariance of the data through a few modes of variability. The modes that account for the largest percent of the original variability are retained after satisfying the traditional statistical significance tests. These modes can be represented by orthogonal spatial patterns (eigenvectors) and corresponding time series (principal components) (Peixoto and Oort, 1992). The EOF is applied to the monthly/pentad CMAP data and NCAR-CAM2.0.1 model rainfall data. The method allows us to extract significant trends found in both data sets. The EOF is not applied to the FVGCM scenario. Instead we use the typical IPCC method of diagnosing spatial pattern changes by subtracting the 1961-1990 FVGCM seasonal rainfall average from the projected 2071-2100 seasonal rainfall average.

3. Results and Discussion

In this section we will describe first the rainfall and hydrological trends during OND season. The rainfall trends are diagnosed from CMAP seasonal, pentad and monthly EOF, seasonal discharge from the White and Blue Nile Rivers, and projected rainfall changes from NCAR/NASA-CCM3 A2 scenario. We will also describe temperature trends from the Climate Research Unit temperature, NCAR–CAM2.0.1 GHA averaged temperature, and projected temperature changes from NCAR/NASA-CCM3 A2 scenario.

3.1 Rainfall Trends

3.1.1 CMAP

EOF analysis was performed on seasonal average of monthly CMAP data, monthly CMAP data and pentad CMAP data to extract possible rainfall trends during the recent decades (1979-2001). The GHA area enclosed in the analysis include Burundi, Djibouti, Eritera, Ethiopia, Kenya, Rwanda, Somalia, Sudan, Uganda, and Tanzania. The domains for the monthly and pentad EOF are similar, but slightly different because we wanted to address the sensitivity of the EOF to domain size, 13.75°S-16.25°N, 21.25°E-53.75°E for pentad compared to 12°S-12°N, 24.0°E-48.0°E for the monthly and seasonal analysis. As we will demonstrate, the EOF in this case is not sensitive to the domain size because we retrieve similar EOF patterns and time series. The first EOF mode characterizes the interannual variability of El Nino Southern Oscillation (ENSO) and a co-existing Indian Ocean Zonal Mode (IOZM) during the OND season over the GHA. This study is an investigation of decadal trends, and therefore, we will not discuss this mode of variability. For more details 0see Schreck and Semazzi (2004) and Bowden and Semazzi (2005). The second EOF mode characterizes a decadal rainfall trend. Schreck and Semazzi (2004) note that most of the previous studies did not include the recent decades since the late 1970s when unusually rapid warming has been in progress, in contrast to the decades of the 1940s through to the late

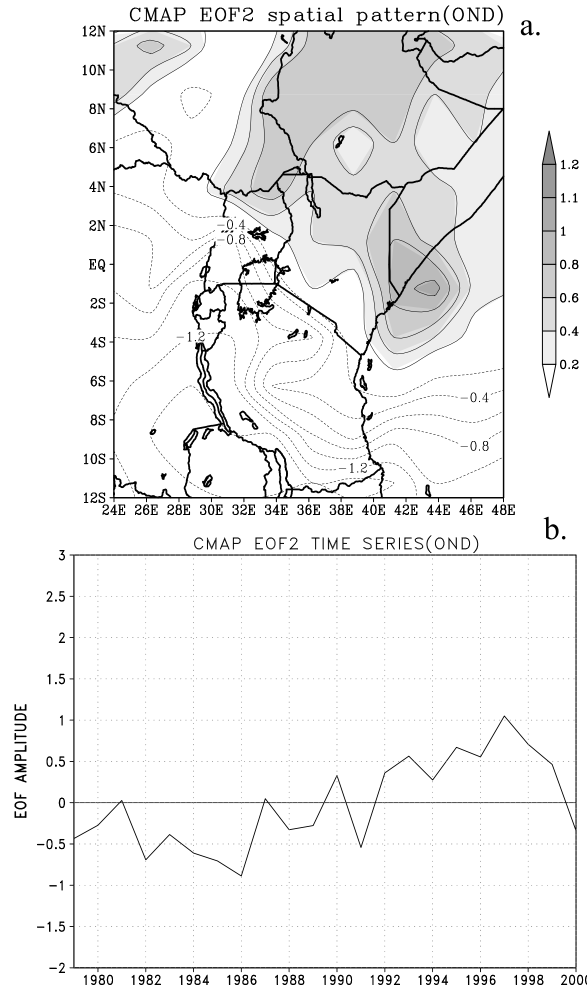

FIG. 2: a) Seasonal EOF2 loading pattern. b) Seasonal EOF2 time series.

1970s when no appreciable changes in global average surface temperature occurred. One primary objective of this study is to investigate the decadal rainfall trend of the recent decades in relationship to global warming and other possible physical processes. We will also diagnose the intraseasonal variability of the trend from the pentad analysis.

Figure 2a displays the spatial pattern for seasonal CMAP EOF2, which explains 14% of the total variance. The distribution of the loadings is characterized by a dipole loading pattern. The corresponding time series (Figure 2b) exhibits both strong interannual variability and low-frequency background variability. The evolution of the background amplitude reached its lowest levels during the early 1980s and peaked in the mid-1990s, and overall there is an increasing trend during the entire period. There is indication of subsequent decline in the amplitude during the late-1990s. Combined interpretation of the distribution of loadings and the corresponding time series suggests that northern sector of GHA is getting wetter while the southern sector is drying up. Inspection of the time series suggests a relationship with global warming (Schreck and Semazzi 2004).

The intraseasonal variability will be diagnosed in two ways. The first inspection is via individual monthly CMAP EOFs, while the other inspection is based on pentad CMAP EOF. We first show in table 1 the fraction (%) of the total rainfall variance accounted for by the two leading eigenmodes for all months in the monthly analysis and the seasonal pentad analysis.

Figures 3a, 3b and 3c illustrate rainfall loading patter over the north/south of the equator for the monthly EOF. The time series for the individual months (Figures 3d, 3e, 3f) demonstrate a quasi-decadal trend in the rainfall anomalies over the GHA, similar to the seasonal analysis. The positive dipole structure (positive anomalies) propagates southward during the season with an orientation northwest to southeast. Also, there are two positive loading maximums, one near coastal Kenya and the other maximum in the interior GHA centered in Ethiopia (October) and Sudan (November/December). It is hard to draw a relative conclusion of the intraseasonal strength of the trend because of the numerous spatial patterns and time series. To address this issue we perform EOF over the season on pentad CMAP data. This allows us to examine the relative strength of the intraseasonal trend. Basically, we can determine which month the trend is the strongest. Figure 4a illustrates the spatial pattern for pentad analysis. Again, there is a dipole loading pattern north/south of the equator. The positive loadings are located over northern Somalia with the largest negative loadings situated southeast of Lake Victoria. Notice that there are no longer two maximum as in the monthly analysis. This is consistent because the seasonal pentad analysis is an average pattern of the individual months. The pentad time series (Figure 4b) in comparison to the seasonal analysis is similar with a pronounced decadal trend. Rearranging the pentad CMAP EOF2 time series (Figure 5) illustrates the relative strength of the intraseasonal trend in comparison to the monthly analysis. The years are arranged in consecutive order (1979-2001) for each pentad of every month. Each pentad has 23 years with six pentads per month. Overall, the time series represents the trend for each pentad within the season. It is important to note that the pattern changes in time as seen in Figure 3. Largest negative anomalies occur during the early decade of the 1980's and largest positive anomalies during the past decade. The intraseasonal monthly time series depicts October as having the strongest trend mode. Each pentad within October exhibits a decadal trend. The largest trends occur during the last three pentads of October. These pentads have positive and negative anomalies which are as large as two standard deviations. The months of November and December have a weaker trend mode. The weakest trend is during the middle of November with the third pentad having small to no trend. By the end of November into December the trend is more pronounced with positive and negative anomalies reaching two standard deviations. Overall, the strongest intraseasonal variability of the decadal trend is during October. This is the onset month of the rainy season for much of GHA. In conjunction with the spatial pattern, the northern portions of GHA (Somalia, eastern Ethiopia, and northern Kenya) experience an increasing trend in rainfall over the past two decades. We suggest that the increasing trend is possibly related to an early onset of the rainfall over the region. The southern portion of GHA (southern Keya, Tanzania, Uganda, Congo tropical rainforest, western Sudan) experience decreasing trend in rainfall possibly related to a late start in the seasonal rainfall. The presence of the trend in November and December suggest weaker but similar rainfall patterns.

3.1.2 Nile Basin

The variability of the White Nile and Blue Nile has distinct similarities and differences as illustrated in Figure 6. The similarities occur about the interannual variability. For example, the large above normal discharge, hence above normal rainfall, of 1916 and 1917 are clearly seen in both rivers. Despite the agreement in the interannual variability, the two rivers have trends of opposite nature. The Blue Nile river tended to have a smaller discharge during the later part of the century (1970s) compared to the earlier part of the century (1910s). The opposite is true for the White Nile, except for the large events of 1916 and 1917. The two source regions for the White Nile/Blue Nile occur in the negative/positive regions of CMAP EOF2. From this we infer that during the recent decades (1980-2000), the rainfall trend has switched sign with more rainfall (discharge) along the Blue Nile and less rainfall (discharge) along the White Nile. We recognize that this inference may be flawed because the rivers are also sensitive to environmental factors

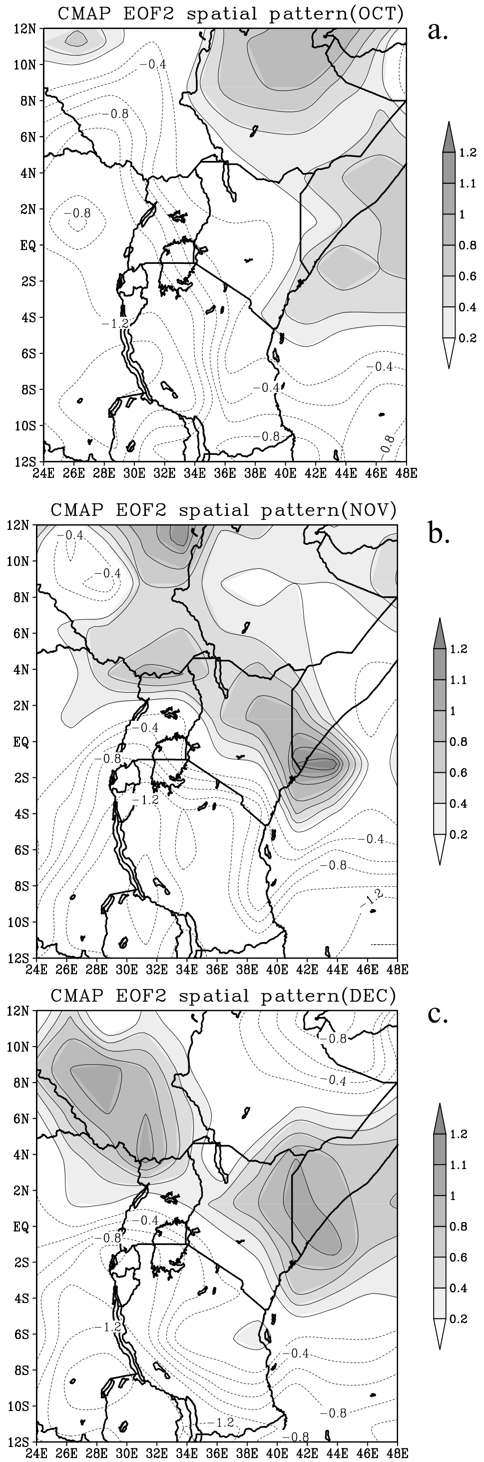

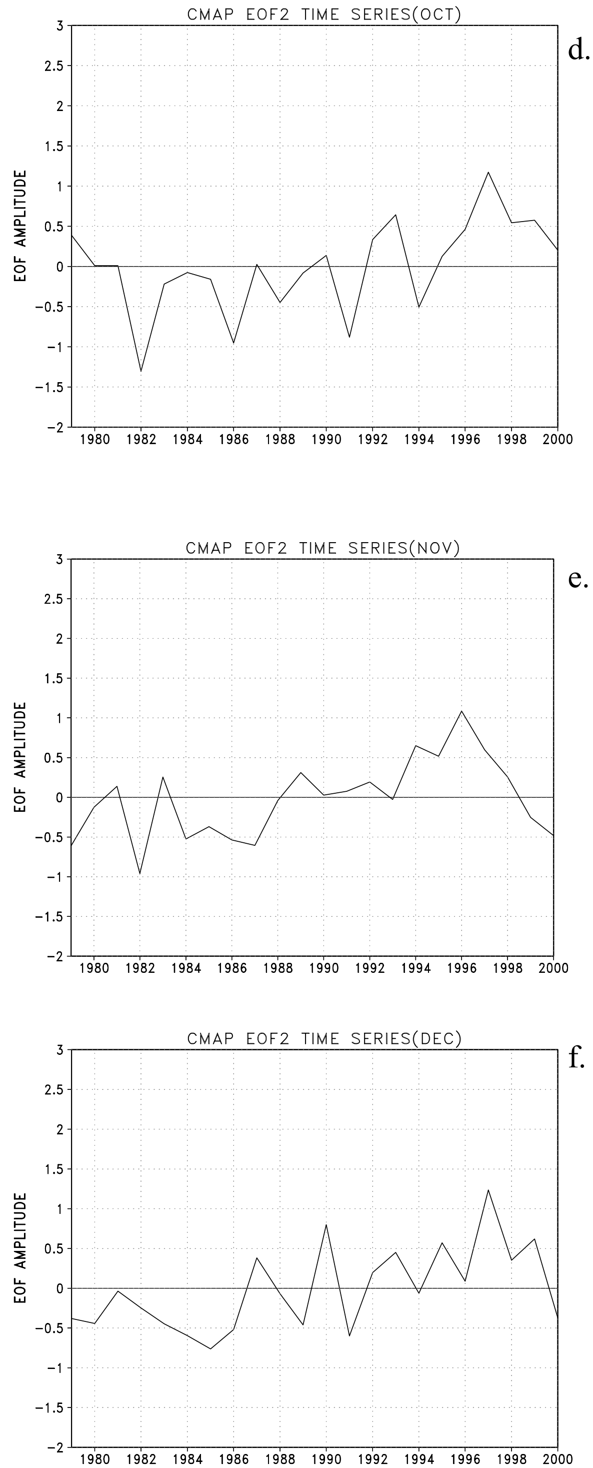

FIG. 3: a) EOF 2 loading pattern for October. b) EOF 2 loading pattern for November. c) EOF2 loading pattern for December. d) EOF2 time series for October. e) EOF2 time series for November. f) EOF2 time series for Decemeber.

OCT – Monthly EOF2	17% Total Variance
NOV – Monthly EOF2	13% Total Variance
DEC – Monthly EOF2	16% Total Variance
OND – Monthly EOF2	15% Total Variance
OND – Pentad EOF2	8% Total Variance

Table 1: Percent variance of total rainfall for monthly and pentad EOF analysis.

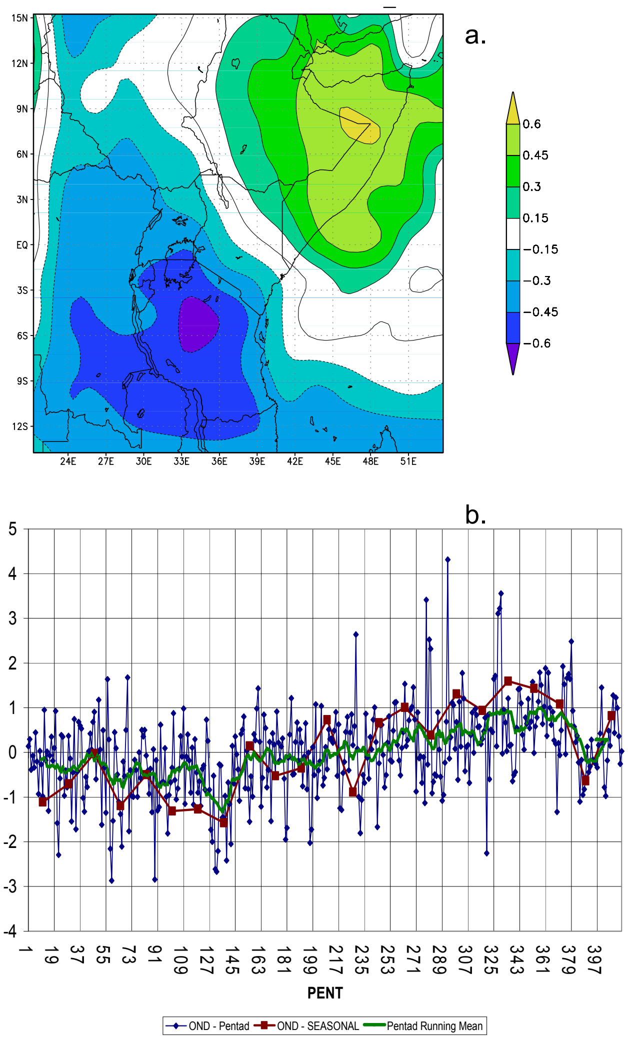

FIG. 4: a) Pentad EOF2 loading pattern. b) Pentad EOF 2 time series (blue), pentad running mean (green), monthly seasonal EOF2 (burgundy).

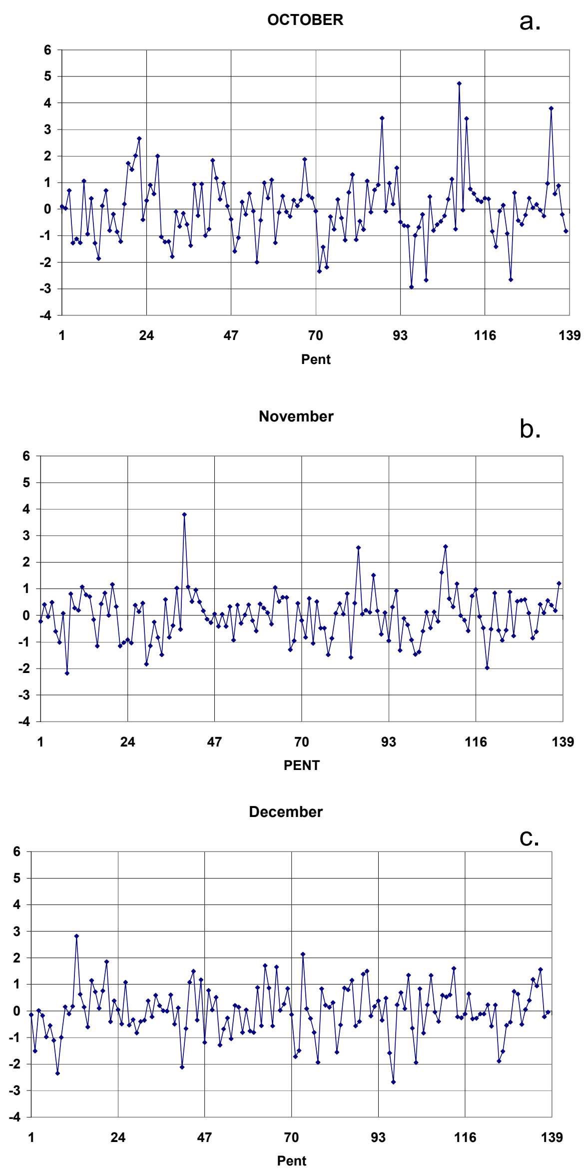

FIG. 5: : Intra-seasonal variability of the decadal trend for a) October b) November c) December. The x-axis gridlines represents the beginning of a new pentad. Each pentad contains the Pentad CMAP EOF2 amplitudes in order from 1979-2001.

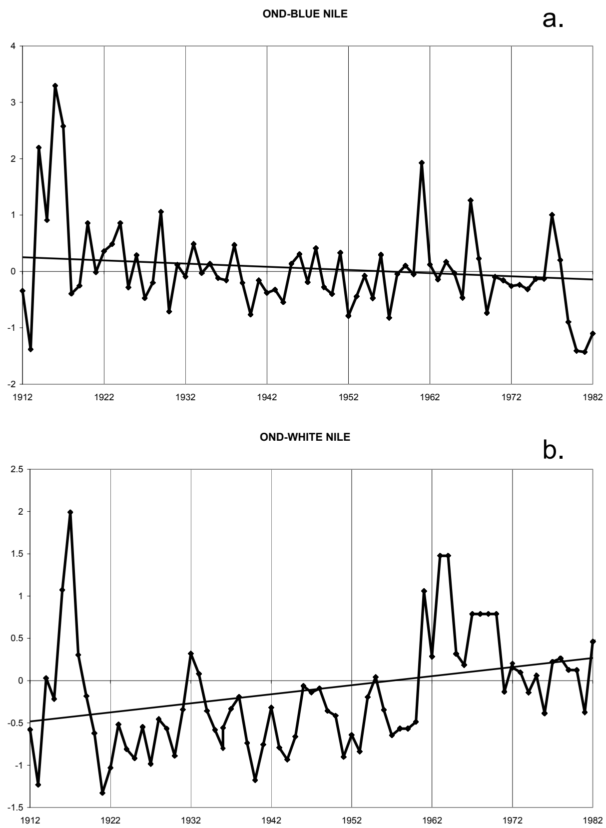

FIG. 6: Seasonal normalized average of river discharge from 1912-1982 for a) Blue Nile b) White Nile.

such as temperature and the inherent runoff due to melting of snow. Also, the results suggest that the recent trend found in CMAP may be representative of natural multidecadal variability, which in itself may be amplified in the presence of global warming. Future research of the discharge trends will take into account the complex interaction between rainfall, temperature change and runoff using a hydrological model.

3.1.3 NCAR-CAM2.0.1

The NCAR-CAM2.0.1 is deficient in resolving the latitude-time evolution of rainfall pattern over GHA; therefore the intraseasonal variability is not well resolved in the NCAR-CAM2.0.1. Fortunately, the model performs well with respect to the seasonal mean (Anyah 2005). Performing EOF on NCAR-CAM2.0.1 seasonal mean rainfall demonstrates the models ability to capture the dominant modes of variability, ENSO and decadal trend, respectively. In order to diagnose distinct trends in rainfall over the GHA, the dominant effects of ENSO on the interannual variability of the regional climate have been filtered out in the EOF2 time series. The second mode of variability accounts for about 18% of the total rainfall variance. Similar to the pattern derived from observed data, the spatial pattern (Figure 7a) is characterized by positive loadings over many parts of Kenya, western Uganda, southwestern Ethiopia, and Somalia. On the other hand, most areas south of the equator that includes central and southern Tanzania are shown to experience negative loadings. Figure 7b show the time series of the 5-year running mean of NCAR-CAM2.0.1 for the seasonal mean ensemble average (40 years, 1961-2000), gauge observations (30 years; 1961-1990) and CMAP (22 years; 1979-2000). Different time

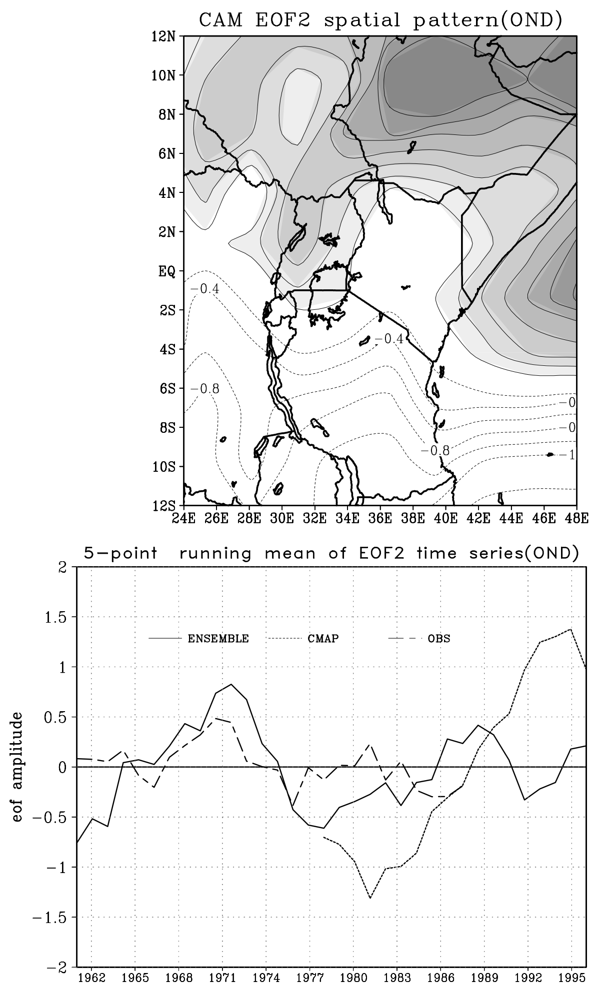

FIG 7: a) CAM2.0.1 EOF 2 spatial pattern (1961-2000) b) 5-point running mean of EOF2 time series of CAM2.0.1 ensemble average, CMAP and gauge observations over East Africa.

periods are used in the three data sets due to discontinuities in the observations and other proxies such as CMAP. Hence, it was not possible to perform EOF analysis over a synchronized time period for all datasets. The seasonal mean anomalies are characterized by three distinct quasi-decadal regimes. The first regime (1961-1971) has an increasing trend.
The second regime (1971-1978) shows a decreasing trend and the third (1982-1994) show persistent increase in rainfall anomalies. These results are in agreement with an earlier study by Schreck and Semazzi (2004), which showed increasing trend in rainfall anomalies over the GHA from mid 1980s through later 1990s matched with the trend of the mean surface temperature anomalies. While their suggestion that the trend could be a regional footprint of global warming remains plausible, our analysis of data extended back in time show the quasi-decadal trend in rainfall anomalies are characterized by both decreasing and increasing regimes as opposed to mean surface temperature anomalies which show a steady increase since 1961. Hence, the trend in the rainfall anomalies over the GHA is not necessarily concomitant with mean surface temperature anomaly trends. Bowden and Semazzi (2005) illustrate that the observed rainfall anomalies of CMAP EOF2 more closely follow the Atlantic Multidecadal Oscillation Index (AMO), which expresses area average SST north of the equator (0°-70°N). Previous studies have shown the existence of decadal rainfall fluctuations over the entire African continent with relationships tied to the Atlantic Ocean (Nicholson, 1996; Semazzi et al., 1996) with marked fluctuations over the Sahel (Folland et al., 1991, Rowell et al., 1992, among others). It is important to note that the AMO index may also mask possible warming due to anthropogenic activities during the recent decades. The hydrological trends over the Nile Basin also suggest that the trend may be associated with natural variability.

3.1.4 NCAR/NASA-CCM3

NCAR/NASA-CCM3 is able to represent the climatological rainfall pattern over the GHA (Anyah 2005). Our main objective is to use the projected A2 IPCC scenario to diagnose rainfall pattern change. Notice that we subtract the control (1961-1990) from the A2 scenario projection (2071-2100)l. We can not diagnose these results with respect to what one may expect based on present day EOF trends because all the variance is accounted for in this pattern. Future EOF will be applied to the IPCC A2 scenario rainfall data in order to address this question.

Figure 8 is an illustration of the A2 IPCC rainfall pattern changes. There are several regions based on this projection that will receive a significant increase in the seasonal rainfall amounts with maximum amounts exceeding 400mm. These areas include western Kenya, Lake Victoria basin, northern Tanzania, and northern Somalia. There are also regions that will receive a significant decrease in precipitation including Democratic Republic of Congo, eastern Kenya and southeastern Somalia. Regions of the Democratic Republic of Congo may expect rainfall to decrease in excess of 200mm. The sense of the rainfall pattern changes is a northeast to southwest dipole, similar to observed EOF2. It is important to remember that the projection includes all the variance including ENSO, which is the dominating mode of variability for the region; therefore, future EOF on the projected rainfall will be helpful when comparing with observed trends. Also, the precipitation pattern does not show any elevation dependence as one may expect based on the findings of Giorgi et al (1997). Rather a rainfall maximum is found over Lake Victoria. Sensitivity study of surface temperatures of Lake Victoria by Anyah and Semazzi (2004) conclude that warmer lake surface temperatures result in increased rainfall over the lake basin. Such a change may have

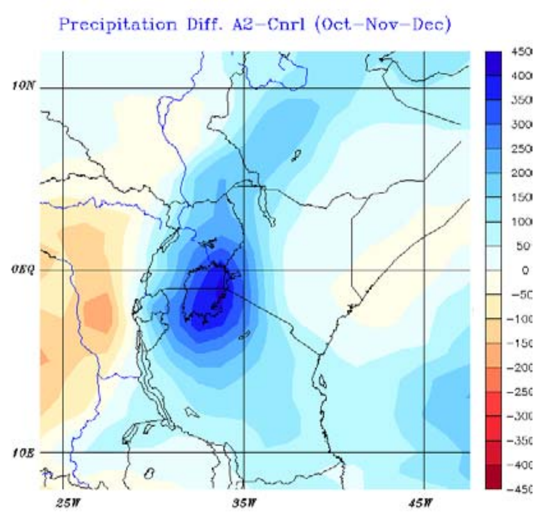

FIG. 8: NCAR/NASA-CCM3 IPCC A2 precipitation changes (IPCC A2 scenario minus control).

substantial impact on hydroelectric power, fisheries, and other socio-environmental activities over the GHA.

3.2 Temperature Trends

3.2.1 NCAR-CAM2.0.1

In figure 9a-d we compare the spatial averages of CAM2.0.1 and observed (CRU) mean monthly surface temperatures. The spatial averaged values were computed over central parts of East Africa bounded within 28°E and 39°E longitudes, 4°N and 4°S latitudes. In figure 7a, the 40-year (1961-2000) time series of the normalized spatial average of monthly mean surface temperature in October for both CRU and the ensemble average show a consistent increasing trend. However, despite the close resemblance in the interannual variability of the normalized surface temperature, the correlations between the GCM ensemble average and CRU data are quite modest over both regions 0.62, though significant at 95% confidence level. However, despite showing a similar trend as CRU data, the GCM ensemble average surface temperatures are also consistently warmer by about 3°C throughout the 40-year period. Similar warming trend is shown in November (Figure 7b). The warming is particularly more pronounced during the last two decades of the time series (1980-2000). A slight decrease (cooling) in the surface temperature during the first decade in the series (1961-1970) is also apparent in both ensemble average and CRU observed surface temperatures. In December, the fluctuations of the mean surface temperatures above/below the long-term mean are relatively smaller in both the GCM ensemble

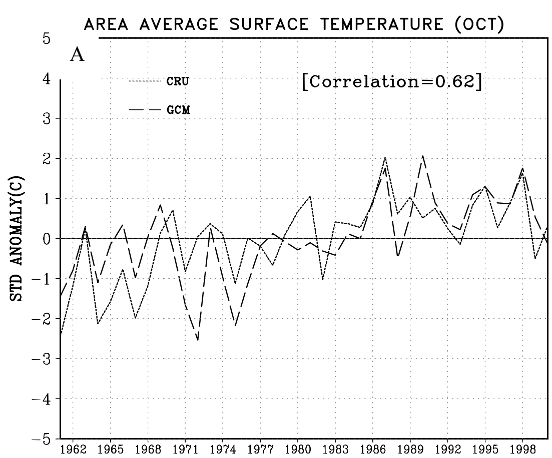

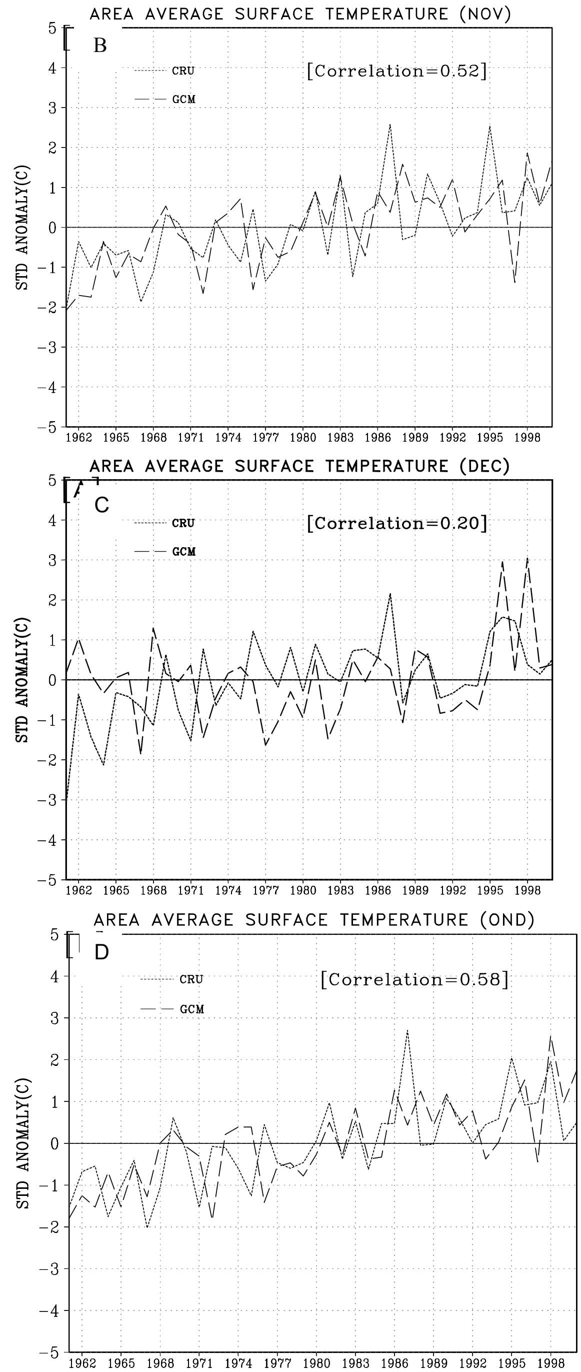

FIG. 9: Comparison of normalized monthly mean surface temperature between CRU and NCAR-CAM2.0.1 ensemble average for a) October b) November c) December d) season-OND

average and observations. Besides, no distinct periods of increasing/decreasing trend are present in the 40-year time series. The correlation between the time series is nevertheless exceptionally low, less than 0.3. On the other hand, the seasonal mean surface temperature generally show a warming trend, with the period between 1980-2000 showing fluctuations of about 1 standard deviation above the mean in both ensemble and CRU datasets.

3.2.2 NCAR/NASA-CCM3

The IPCC A2 scenario projected temperature (2071-2100) minus the control (1961-1990) is illustrated in Figure 10. The projection indicates that the entire GHA will experience warming with minimal warming values around 2°C. The largest projected warming occurs over the higher elevations of East Africa and Ethiopia with warming over 3.5°C. This is consistent with previous study of Giorgi et al. (1997). Their study used a projected CO2 experiment over the Alpine region. They found the surface temperature was elevation dependent resulting in more pronounced warming at higher elevations compared to low elevations attributed to depletion of snowpack and enhanced snow-albedo feedback. Changes in surface energy and water budgets may also play a role in the warming elevation dependence. The warming at the higher elevations is crucial for GHA because many of the cash crops such as tea and coffee are grown in the highland regions. Small changes in temperature or precipitation may alter the productivity and sustainability of the cash crops.

4.0 Conclusions

This study investigated various trends in precipitation and temperature including observed, modeled and model projected trends. The precipitation patterns of the recent decades, which were diagnosed using EOF analysis, depict that northern GHA is becoming increasing wetter while southern GHA is becoming drier. Intraseasonal variability of the trend using monthly analysis illustrates that the dipole like rainfall anomalies are spatially complex when considering the evolution of the trend. The trend is found to be strongest during October which is important because this is the onset month of the rainy season for the majority of the GHA. The EOF analysis from CAM2.0.1 suggests that the dipole rainfall anomalies are part of a quasi-decadal trend. Hence, the trend in rainfall anomalies over the GHA is not necessarily concomitant with mean surface temperature anomaly trends. The hydrological trends agree with these findings in that the region may be experiencing climate change due to inherent natural multidecadal variability, which in itself may mask global warming. The projected rainfall based on the IPCC A2 scenario favors a northeast to southwest dipole, similar to observed EOF2. The largest change in precipitation is found over the Lake Victoria basin. The increased precipitation over Lake Victoria is important for many socio-economic sectors including hydroelectric power and fishereies.

The seasonal mean surface temperature generally show a warming trend, with the period between 1980-2000 showing fluctuations of about 1 standard deviation above the mean in both ensemble NCAR-CAM2.0.1 and CRU datasets. As for the projected surface temperature, based on the IPCC A2 scenario, the temperature changes were found to be elevation dependent with higher elevations warming faster than the lower elevations. The warming of high elevations can exceed 3.5°C. Such drastic warming over the next 100 years could alter the productivity of many cash crops over the highland areas of the GHA.

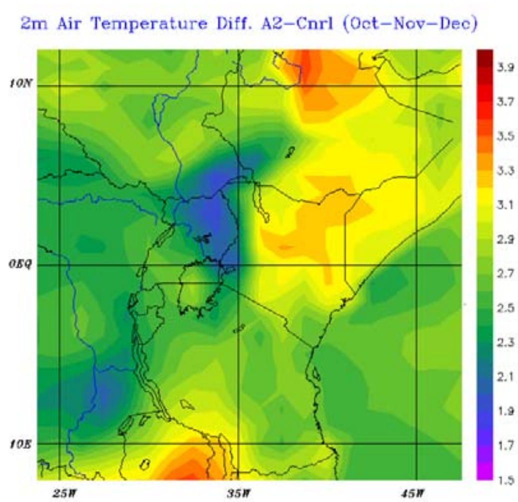

FIG. 10: NCAR/NASA-CCM3 IPCC A2 temperature changes (IPCC A2 scenario minus control).

References

Anyah, R.O., 2005: Modeling the variability of the climate system over the Lake Victoria basin. PhD. Thesis, North Carolina State University, USA, 305pp.

Anyah, R.O., and F.H.M. Semazzi, 2004: Simulation of the response of Lake Victoria basin climate to lake surface temperatures. *Theor. Appl. Climtol.*, 79,55-69.

Bowden J., and F.H.M. Semazzi, 2005: Empirical analysis of the intraseasonal variability over the Greater Horn of Africa. *Submitted, Theor. Appl. Climatol.*

Coppola, E., and F. Giorgi, 2005: Climate change in tropical regions from high resolution time slice AGCM experiments. *Submitted. Quar. J. R. Met Soc.*

Folland, C.K., J.A. Owen, M.N. Ward, and A.W. Colman, 1991: Prediction of seasonal rainfall in the Sahel region using empirical and dynamical methods. *J. Forecasting*, 10, 21-56.

Giorgi, F. J. Hurrell, M.R. Marinucci, and M. Beniston, 1997: Elevation dependency on the surface climate change signal: A model study. *J. of Clim.*, 10, 288-296.

Hastenrath, S. and L. Greischar, 1997: Glacier recession on Kilimanjaro, East Africa, 1912-1989. *J. Glaciology*, 43: 455-459.

Intergovernmental Panel on Climate Change (IPCC), 1998: The regional impacts of climate change: An assessment of vulnerability. *Special Report of IPCC Working Group II. IPCC.* Cambridge University Press, Cambridge, United kingdom and New York, NY, USA, 880pp.

Lin, S.J. and R.B. Rood, 1996: Multidimensional flux form semi-lagrangian transport schemes. *Mon. Wea. Rev*., 124, 2046-2070.

Lin, S.J., 2004: A vertically langrangian finite-volume dynamical core for global models. *Mon. Wea. Rev.,*132, 2293-2307.

New, M., M. Hulme, and P. Jones, 1999: Representing twentieth-century space-time climate variability. Part 1: Development of a 1961-1990 mean monthly terrestrial climatology. *J. Climate*, 12, 829-856.

Nicholson, S.E. 1996: A review of climate dynamics and climate variability in Eastern Africa. *The Limnology, Climatology, and Paleoclimatology of the East African Lakes*. Gordan and Breach, New York 57pp.

O' Reilly, C., S. R. Alin, P-D Plisnier, A.S. Cohen, B. A. McKee, 2003: Climate change decreases aquatic ecosystem productivity of Lake Tanganyika, Africa. *Nature*, 14, 766-768.

Peixoto, J.P. and A.H. Oort, 1992: *Physics of Climate*. American Institute of Physics, NY. Pp. 492-496.

Rowell, D.P., C.K. Folland, K. Marskell, J.A. Owen, and M.N. Ward, 1992: Modelling the influence of global sea surface temperatures on the variability and predictability of seasonal Sahel rainfall. *Geophy. Res. Lett.*, 19, 905-908.

Schreck, C.J. and F.H.M. Semazzi, 2004: Variability of the recent climate of Eastern Africa. *Int. J. Climtol*., 24, 681-701.

Semazzi, F.H.M., B. Burns, N.H. Lin and J.E. Schemm, 1996: A GCM study of the teleconnections between the continental climate of Africa and global sea-surface temperature anomalies. J. Climate, 9, 2480-2497.

Serageldin, I. 1995: Nurturing Development (Aid and Cooperation in Today's Changing World). The World Bank, Washington, DC, USA.

Simmons, A.J. and R. Stufing, 1981: An energy and momentum conserving vertical finite difference scheme, hybrid coordinates and medium range weather prediction. Tech Report ECMWF, Report No. 28, Europoean Center for Medium Range Weather Forecasts, Reading UK: 68pp.

Xie, P. and P.A. Arkin, 1995: An intercomparison of gauge observation and satellite estimates of monthly precipitation. *J. App. Met*. 34, 1143-1160.

Xie, P. and P.A. Arkin, 1997: Global Precipitation: a 17 year monthly analysis based on gauge observations, satellite estimates, and numerical model outputs. *Bull. Amer. Met. Soc*., 78, 2539-2558.

Xie, P., J.E. Janowiak, P.A. Arkin, R. Adler, A. Gruber, R. Ferraro, G. J. Huffman, S. Curtis, 2003: GPCP pentad precipitation analysis: An experimental dataset based on gauge observations and satellite estimates. *J. Climate*, 16, 2197-2214.

Zhang, G.J., and N.A. McFarlane, 1995: Sensitivity of climate simulations to the parameterization of cumulus convection in the CCC-GCM. *Atmos.-Ocean*, 3, 407-446.